

Journal of Photonics for Energy

PhotonicsforEnergy.SPIEDigitalLibrary.org

Photophysics of organic photovoltaic devices: a review

Chengxi Zhang
Rugeng Liu
Chun Hong Mak
Xingli Zou
Hsin-Hui Shen
Shao-Yuan Leu
Li Ji
Hsien-Yi Hsu

SPIE.

Chengxi Zhang, Rugeng Liu, Chun Hong Mak, Xingli Zou, Hsin-Hui Shen, Shao-Yuan Leu, Li Ji, Hsien-Yi Hsu, "Photophysics of organic photovoltaic devices: a review," *J. Photon. Energy* **8**(2), 021001 (2018), doi: 10.1117/1.JPE.8.021001.

Photophysics of organic photovoltaic devices: a review

Chengxi Zhang,^{a,b} Rugeng Liu,^{a,b} Chun Hong Mak,^{a,b} Xingli Zou,^c
Hsin-Hui Shen,^d Shao-Yuan Leu,^e Li Ji,^{f,*} and Hsien-Yi Hsu^{a,b,*}

^aCity University of Hong Kong, School of Energy and Environment, Kowloon, Hong Kong SAR, China

^bShenzhen Research Institute of City University of Hong Kong, Nanshan District, Shenzhen, China

^cShanghai University, State Key Laboratory of Advanced Special Steel and School of Materials Science and Engineering, BaoShan District, Shanghai, China

^dMonash University, Department of Materials Science and Engineering, Faculty of Engineering, Clayton, Victoria, Australia

^eHong Kong Polytechnic University, Department of Civil and Environmental Engineering, Hung Hom, Kowloon, Hong Kong SAR, China

^fUniversity of Texas at Austin, Microelectronics Research Center, Department of Electrical and Computer Engineering, Austin, Texas, United States

Abstract. The field of organic solar cells (OSCs) has developed rapidly over the last two decades, and polymer solar cells with power conversion efficiencies of 13.1% have been reported. The understanding of the photophysical mechanisms in photovoltaic devices plays a significant role in determining the optoelectronic properties of high-performance OSCs. This review gives a fundamental description of the photophysical mechanisms in OSCs, with the main emphasis on the exciton transfer and charge-transfer mechanisms. In addition, it highlights the capabilities of various experimental techniques for the characterization of energy transfer and charge transport, as well as their roles in dictating the architecture of photovoltaic devices. © 2018 Society of Photo-Optical Instrumentation Engineers (SPIE) [DOI: [10.1117/1.JPE.8.021001](https://doi.org/10.1117/1.JPE.8.021001)]

Keywords: organic photovoltaics; photophysics; exciton transfer; charge transport.

Paper 18052MV received Mar. 7, 2018; accepted for publication May 22, 2018; published online Jun. 9, 2018.

1 Introduction

One of the most promising ways to tackle today's energy issues and meet the world's large energy demand is harnessing solar energy intelligently and efficiently. Solar cells, which convert the sunlight directly into electricity by the photovoltaic effect, are one of the fast-growing technologies for harvesting solar energy. Solar cells based on the use of inorganic materials, such as crystalline silicon (Si), cadmium telluride (CdTe), or copper indium germanium selenide (CIGS), have become dominant photovoltaic technologies in recent years. However, the high cost of raw materials and manufacturing processes have impeded the pace of development of solar cells. Thus, we are stimulated to explore low-cost and environmental-friendly materials for solar cell devices. In the last two decades, organic solar cells (OSCs), especially polymer solar cells, have attracted a significant amount of attention and developed rapidly due to their advantages of being low-cost, lightweight, and easily fabricated in large areas by roll-to-roll techniques.¹⁻³ Tang⁴ successfully introduced the donor-acceptor bilayer planar heterojunction to organic photovoltaic cell by utilizing copper phthalocyanine and perylene tetracarboxylic derivative as materials for Frenkel exciton formation, dissociation, and transportation. This two-layered organic photovoltaic cell achieved a low power conversion efficiency (PCE) of

*Address all correspondence to: Li Ji, E-mail: nmgjili@utexas.edu; Hsien-Yi Hsu, E-mail: sam.hyhsu@cityu.edu.hk

about 1% and fill factor (FF) value as high as 0.65 under simulated AM2 solar illumination. One of the milestones in OSCs was the wide application of fullerene and its derivatives (such as [6,6]-phenyl-C₆₁-butyric acid methyl ester, PCBM) as electron transport materials in OSC devices. A few years later, Sariciftci et al.⁵ and Kraabel et al.⁶ observed the photo-induced electron transfer phenomena from poly[2-methoxy-5-(2-ethylhexyloxy)]-1,4-phenylenevinylene (MEH-PPV) and fullerene (C60) composite, which showed the successful application of donor and acceptor materials in OSC devices and realized the efficient electron transfer into the electrode. Sariciftci et al.⁷ first demonstrated the planar heterojunction polymer solar cells; however, the small contact area between the donor–acceptor interface and shorter hole and electron carriers diffusion lifetime limited the development of this type of OSCs. These issues were addressed later by codepositing p-type phthalocyanine (PC) pigments and n-type perylene derivative (PTC) pigments to form a sandwich-like three-layered OSC.⁸ The bulk heterojunction (BHJ) that involves mixing donor and acceptor in the bulk body of OSC devices realized a large number of molecular interface contacts for effective charge carrier photogeneration. Halls et al.⁹ and Yu et al.¹⁰ developed an efficient BHJ polymer solar cell that achieved charge separation efficiently due to the photo-induced electron transfer from donor material (MEH-PPV) to acceptor material (C60). Since then, the polymer-fullerene and BHJ structure became the standard configuration for the development of organic polymer solar cells. Recently, Zhao et al.¹¹ reported a highly efficient PBTA-TF:IT-M-based device that was processed by environmentally friendly solvents, tetrahydrofuran/isopropyl alcohol (THF/IPA) and *o*-xylene/1-phenylnaphthalene; state-of-the-art OSCs could achieve a top conversion efficiency of 13.1%. Furthermore, the PCE of THF/IPA-processed large-area device (1.0 cm²), which was made by blade-coating techniques, could maintain at 10.6%, driving leapfrog development of large-scale production of high-efficient OSCs in the near future.

Until now, the field of OSCs has experienced significant growth, and the mysterious photoelectricity conversion mechanisms were unveiled gradually in the past 30 years. It is clear that the photoelectricity conversion process in OSCs can be summarized in three crucial points: (1) exciton generation, transport, and dissociation; (2) charge carrier transport; and (3) charge carrier collected by electrodes.¹² However, the fundamental understanding of relevant physical dynamics in OSCs should be improved for designing the next generation of photovoltaic materials and devices.

The goal of this review is to provide a wide scope and recent advanced understandings toward the photophysical mechanism, which is a decisive factor in obtaining high-performance OSC devices. In this review, the simple models and underlying energy transfer mechanisms of exciton generation, transport, and dissociation are introduced. In the subsequent part, the mechanisms of charge carrier generation, transfer, trapping, and recombination in OSCs are described in detail. Then, the characterization techniques for the photophysical dynamics in OSCs are presented. In addition, a brief summary and future perspectives for OSC devices are discussed.

2 Exciton Energy Transfer

For organic semiconductor materials, the highest occupied and the lowest unoccupied molecular orbitals (HOMO and LUMO, also can be denoted as π and π^* , respectively in π -systems) have huge effects on electrical conductivity and optical properties. In the ground state, electrons fill orbitals with lowest energies by maximum two electrons with the spins in opposite directions at each orbital. The bandgap value, which is the important parameter of organic semiconductor materials, can be obtained from the energy difference between HOMO and LUMO energy levels.¹³ If the electron originated from a molecule is bouncing to get rid of the exciton binding force due to the absorption of a photon, the electrons transfer from HOMO to LUMO energy level occurs and then becomes a competing process with the energy transfer (Fig. 1). The wave functions of donor and acceptor materials always determine the short-range interactions (<1 nm), which finally enable the donor and acceptor molecules with positive and negative charges. Marcus theory^{14–16} provided the most common description about the electron transfer from HOMO energy level to LUMO energy level, in which the transfer rate can be expressed as follows:

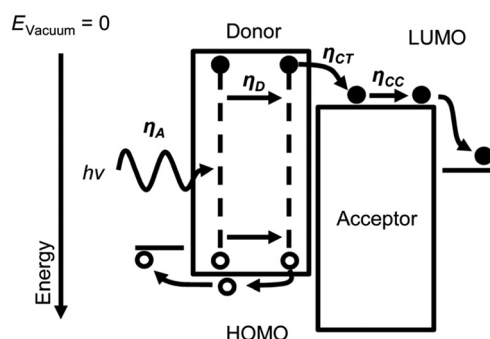


Fig. 1 Simplified schematic of photoconversion in an organic photovoltaic cell with the processes of photon absorption (η_A), exciton diffusion (η_D), exciton dissociation by CT (η_{CT}), and charge carrier collection (η_{CC}) denoted. Reproduced with permission from Ref. 17. Copyright 2013 Royal Society of Chemistry.

$$k_{ET} = \frac{J_{DA}^2}{\hbar} \sqrt{\frac{\pi}{\lambda k_B T}} \exp\left[-\frac{(\lambda + \Delta G)^2}{4\lambda k_B T}\right], \quad (1)$$

where J_{DA} is the electronic coupling, λ is the reorganization energy, and ΔG is the total Gibbs energy change for the exciton transport reaction.

Förster transfer and Dexter transfer are the two main mechanisms for the exciton migration in organic solar devices.^{18–20} The Förster energy transfer, also called Förster resonant energy transfer, occurs with a dipole–dipole electromagnetic interaction when the absorption spectrum of acceptor materials has immense overlap with the emission spectrum of donor materials. The Förster energy transfer phenomenon is commonly observed in the photon absorption and photosynthesis phase, where the energy of absorbed photons is transmitted to the reaction center in the photosensitive materials.

The Dexter transfer occurs when the energy transfers through the direct exchange of electrons if a spectral overlap is presented.¹⁸ The rate of the Dexter transfer becomes negligible as the spacing between donor and acceptor materials reaches more than one or two molecular diameters.²¹ Since the Dexter energy transfer mechanism can be realized through direct exchange of electrons, it requires the spectral overlap between both donor molecules and acceptor molecules. The transfer rate equation for the Dexter energy transfer mechanism can be expressed as²²

$$k_D(d) = KJ e^{\left(-\frac{2d}{L}\right)}, \quad (2)$$

where J is the spectral overlap integral normalized for the extinction coefficient of ground state molecules, K is related to specific orbital interaction, and L is the Van der Waals radius. It is noticeable that the probability of the Dexter energy transfer exponentially decreases with the distance between donor and acceptor.

The Dexter energy transfer is a nearest-neighbor activity with a shorter range of 0.1 to 1 nm, while the Förster energy transfer can occur for donor–acceptor separations in the range of 1 to 5 nm.^{20,23} Since the Dexter energy transfer arises from exchanging electrons of the same spin but different energies, both singlet and triplet excitons may be migrated by this mechanism, whereas only singlet excitons usually can be transferred via the Förster mechanism.^{24,25}

Diffusion is the process that particles in space spread from a high concentration area to a low concentration area with the movement in random directions. The diffusion length is a significant parameter for organic active materials in photovoltaic devices, which reflects an exciton migration distance before it decays. The diffusion length can be described as

$$L_D = \sqrt{ZD\tau}, \quad (3)$$

where D is the diffusion coefficient, τ is the exciton lifetime, and $Z = 1, 2,$ or 3 depending on whether diffusion occurs in one-, two-, or three-dimensional space.

The exciton–exciton annihilation may occur due to high exciton densities. Exciton quenching can also be found by defects, metal interfaces, and so on, leading to the decrease of photoluminescence (PL) lifetimes and quantum yields. Mikhnenko et al.²⁶ reported that the exciton quenching sites for exciton diffusion show the identical origin to traps for charge transport in many polymeric and small-molecule materials. Thus, the optimal charge transport could also be reached by the optimization of exciton transfer. In fact, exciton diffusion coefficients could be increased by reducing the disorder, resulting in the improvement of charge carrier mobility in materials ranging between amorphous polymers²⁷ and crystalline small-molecule films.²⁸

3 Charge Carrier Transport

In OSCs, the excitons (also known as electron–hole pairs) generate through light absorption, which has a relative high binding energy (typically 0.2 to 0.5 eV) due to the Coulombic force attraction. For BHJSCs, the contact interfaces between the donor and acceptor materials become the main sites for dissociating the strongly attracted bound excitons and then form the free charge carriers (hole carrier and electron carrier). When the donor and the acceptor materials contact directly, the electron transfer to the acceptor occurs by overcoming the exciton-binding energy. After this transfer process, Coulombic attraction can affect the electron–hole pairs since the donor and acceptor phases are still physically close to each other. This special temporary phase in which the electron–hole pairs bond by Coulombic attraction is known as the charge-transfer (CT) state.

3.1 Free Charge Generation

The existence of the CT state and ultrafast generation of free charge carriers have been reported; however, it is difficult to figure out how the CT state dissociates into free charge carriers. What is the photophysical mechanism during the transfer process from the CT state to free charge carriers? Is there any controversial debate on the formation of free charge carrier from the hot CT state or the relaxed CT state?

The incident light with photons exceeding the energy of donor material's optical absorption gap will generate a temporary CT state rather than a free charge carrier. During the excitation process, the above-gap excitation and below-gap excitation will appear, but Lee et al.²⁹ have proved that the excess thermal energy plays a negligible role in the CT state separation because these two excitations showed the same short-circuit current of photovoltaic devices by adjusting the incident intensity. At the interface of donor and acceptor materials, the electron will transfer to the acceptor material and leave a hole in the donor material.⁵ It is notable that the singlets will recombine if the path to acceptor materials is too far. The CT state is generally generated with excess thermal energy (ΔG_{CT}) as a result of the energy difference between the excited state and the CT state. At this stage, there are two competing processes, as shown in Fig. 2: (1) the hot CT state generated with excess thermal energy can directly dissociate into charge-separated (CS) states, forming free charge carriers; (2) the hot CT state can thermally relax to the lowest CT state (CT_1) (path 2a) and dissociate to the CS state (path 2b) to generate the photocurrent.³⁰

For the path 1 mentioned above, Ohkita et al.³¹ realized that the excess energy can also result in the formation of free charge carriers before the formation of thermally relaxed charge carrier states. During this internal process, the formation of the hot CT state and dissociation occur with ultrafast conversion time, usually on the order of several hundred femtoseconds.³² The relationship between the excess thermal energy and the formation of free charge carriers has been investigated.³² Clarke et al.³³ found that the short-circuit current based on poly(3-hexylthiophene) (P3HT)/PCBM solar cell has been improved by a simply thermal annealing method. The transient absorption spectroscopy was employed to demonstrate their thermal annealing process, resulting in a twofold increase in the yield of free charge carriers. They ascribed the improvement for the generation of free charge carriers to the increment of the free energy, which is induced by the enhanced polymer crystallinity upon thermal annealing. Their observations well-agree with the hot CT mechanism in which the excess thermal energy enables the

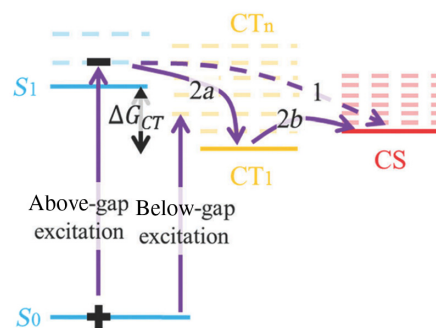


Fig. 2 Energy diagram summarizing the debate concerning charge generation. Photon absorption generates singlet excitons (S_1), which dissociate at the interfaces, forming CT states with excess thermal energy (ΔG_{CT}), known as hot CT states. The hot CT state can (1) directly dissociate into the CS state or (2a) first thermalize to the relaxed CT state (CT_1) and then (2b) dissociate into the CS state. Above-gap and below-gap excitation are also shown in the figure. Reproduced with permission from Ref. 30. Copyright 2014 Royal Society of Chemistry.

electron–hole pairs to overcome their Coulombic binding energy more easily and therefore improves the dissociation efficiency of the CT state. Bakulin et al.³⁴ further investigated the kinetics of the bound CT state and observed that the kinetics of the CT state recombination were quite similar for both charge-generation mechanisms, indicating that the nature of the generated CT states does not depend on the CT pathway. Nonetheless, they found that the yield of bound and free charges strongly depends on the particular driving energy provided by $HOMO_D - HOMO_A$ (hole transfer) or $LUMO_D - LUMO_A$ (electron transfer) of the material system. The yield of bound CT states dramatically increased with decreasing energy difference driving the CT.

Albrecht et al.³⁵ reported that the field dependence of the charge carrier generation mechanism on the photoexcitation of the donor excited state, acceptor excited state, and CT manifold was investigated by the time-delayed collection field technique. The total extracted charge carrier density was detected through measuring the free carrier generation yield at a certain bias voltage. Vandewal et al.³⁶ then confirmed the role of the lowest energy emissive interfacial charge-transfer state (CT_1) during the charge-generation process. They thus demonstrated that free charge carriers can be generated from the relaxed charge-transfer state (CT_1) (path 2) rather than the hot CT state. Howard et al.³⁷ used transient optical spectroscopy in the visible and near-infrared spectral regions to directly observe efficient ultrafast free charge generation in the absence of field in annealed P3HT:PCBM blend. However, they found that the generation of free charge carriers is much less efficient in unannealed and amorphous regiorandom blends with larger ΔG_{CT} . This finding provided additional evidence against the hot CT mechanism in which a larger amount of free charge carriers could be generated by the system with more excess thermal energy. They therefore concluded that the PCE of annealed P3HT:PCBM solar cells depends on their ability to directly generate free charges upon the exciton quenching process. This ultrafast free charge generation highly relied on the surface morphology. The blended films with increased order led to greater free charge generation. By utilizing time-resolved photoemission spectroscopy, Wang et al.³⁸ studied the spatial size and electronic energy of a manifold of CT states at the zinc phthalocyanine (ZnPc)–fullerene (C_{60}) donor–acceptor interface. This investigation provided more detailed information related to the CT process that has not been accomplished by the other experimental techniques. It was found that CT at the interface first populates delocalized CT excitons with the maximum delocalization size of 4 nm. The delocalized CT excitons are then relaxed in energy to produce CT states with delocalization sizes in the range of 1 to 3 nm. While the CT process from ZnPc to C_{60} occurs in about 150 fs after photoexcitation, the localization and energy relaxation occur in 2 ps. This multidimensional investigation on how CT excitons evolve in time, space, and energy could allow us to explore the exciton dissociation mechanism. Recently, Athanasopoulos et al.³⁹ demonstrated that efficient charge separation of electron–hole pairs in organic planar heterojunction solar cells could be achieved by an incoherent hopping process of vibrationally relaxed CT states.⁴⁰ By Monte

Carlo simulations, they simulated the dissociation of the charge-transfer state in polymer–fullerene bilayer solar cells. These theoretical results were then applied to explicate experimental outcomes of field independent charge separation without any “hot” processes, in agreement with Ref. 36. As a result, the coherent transport is not the only pathway to enhance the efficiencies of OSCs. In other words, the performance of organic photovoltaic devices could be optimized by the material architectures through an incoherent hopping mechanism.

3.2 Charge Trapping and Recombination

In conventional crystalline semiconductors, an empty electronic state that is localized and distinct from the delocalized band or transfer states is defined as a trap. For example, an electron trap is an empty state located below the conduction band minimum whereas a hole trap is a state filled with electrons located above the valence band maximum, as shown in Fig. 3. In general, this electronic state has lower energy than the transfer state. It should be noted that the transfer process can be occurred by activated hopping or tunneling from trap to trap if the trap density is high enough. In other words, the trap states are not necessarily immobile.⁴¹

In organic semiconductors, the definition of traps in the band structure of organic materials is the same as the conventional semiconductors in terms of the location of electronic states. The displacement or misorientation of molecules from their equilibrium positions or intramolecular distortions can frequently lead to the intrinsic structural defects of organic semiconductors. If there is enough intermolecular interaction to produce electronic dispersion across molecules in the organic semiconductor, removing a molecule (i.e., creating a vacancy) will reduce the electronic coupling between neighbors and thus increase the electronic energy of electrons and holes. As a result, a vacancy does not give rise to electronic trap states in any distinct way. In a general way, configurations that generate traps must result in an increase in electronic coupling. In general, any irreversible degradation reaction that decreases conjugation or electronic coupling may not create a trap. A portion with a higher-than-average conjugation length can constitute a trap. In organic semiconductor materials, a region of materials where molecules are closer to each other will form a trap region in a thin film. Until now, the structural features with electronic defects in organic semiconductors have not been completely identified and still remained unclear.

In general, the traps in organic semiconductor materials are harmful to the performance of optoelectronic devices. When charges are injected into the semiconductor film, they rapidly thermalize in the density of states (DOS), which possibly involve the traps. Also, the

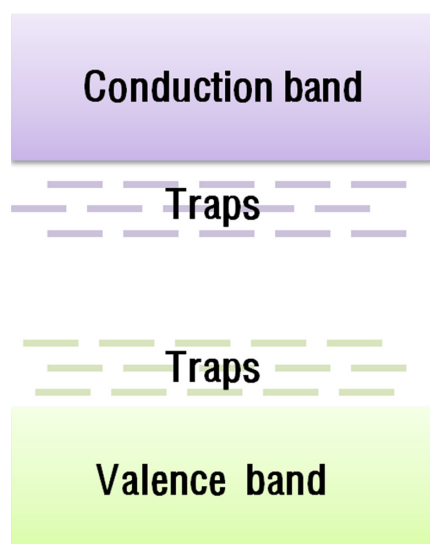


Fig. 3 Sketch of the electronic distribution of trap states in DOS of a semiconductor. Reproduced with permission from Ref. 42. Copyright 2013 Wiley-VCH Verlag GmbH & Co. KGaA.

electrical instabilities on electronic devices may appear when charges relax into traps over longer timescales.⁴² It is fundamentally important to detect and characterize traps in organic materials for establishing structure–property relationships and understanding the origin of electronic defects. In recent years, the optical methods,^{43–45} scanning probe methods,^{46–50} and electrical methods^{51–57} were utilized to detect and probe the origin of traps in organic materials, but the trap distributions still need to be figured out with more advanced techniques and methods.

In OSCs, the CT complex can either be dissociated to yield free charges or recombined to electron–hole pairs. The recombination of CT complexes is either radiative or nonradiative. The electron may be transferred to the ground state, or transferred from acceptor molecules back to donor molecules. In the later case, the photophysical process is from either the regeneration of a donor singlet excited state⁵⁸ or back electron transfer by the transition to a triplet excited state in the donor material.⁵⁹ After a CT complex is generated from a singlet exciton, a subsequent recombination is called geminate because its constituents originate from the same donor excitation.⁶⁰ Thus, it should be a first-order process, showing a lifetime independent of the CT concentration. Nonetheless, CT states are intermediate states as well for the free polaron recombination. When two oppositely charged polarons encounter, they can create a CT complex, which then undergoes a second-order recombination. This is known as nongeminate recombination because the two polarons were formed independently from one another. In general, the probabilities of a recombination process depend on the energy difference between the CT and the overlap integral of the corresponding orbitals.⁶⁰

Another important process related to the CT recombination involves the generation of triplet excitons. Undoubtedly, triplet excited states can be populated not only by intersystem crossing from singlet states of the donors⁶¹ but also by a back electron transfer from a generated CT complex to a triplet exciton again on the donor molecules. These recombination processes for donor–acceptor combinations can result in the degradation of photovoltaic performance. Veldman et al.⁵⁹ systematically studied the relative energies of CT and triplet excited states in the blend of conjugated polymers (as an electron donor) and PCBM molecules (as an electron acceptor) using a combination of electrochemical and photophysical methods. They observed that if the triplet excited state is at least 100 meV lower in energy than the CT state, the recombination process can be easily triggered and further revealed that a singlet–triplet energy gap of $\Delta E_{ST} < 0.2$ eV can prevent the charge recombination into triplet excited states for an optimized organic donor–acceptor heterojunction with a minimal offset between the lowest singlet excited states and CT energies. Hence, the energy level of triplet excited states has to be taken into account to design efficient materials for OSCs with minimal driving force. In general, the recombination from the CT state to triplet state can also be influenced by the electric field. However, this transition process can only take place if the spin dephasing time of the CT state is shorter than its lifetime.⁶² In other words, the recombination occurs if the transfer from the CT state to a triplet state is more rapid than that of its negative constituent into a triplet excited state of the donor. If the relative amount of PCBM molecules is increased, the electron transfer from CT complexes back to triplet excited states is reduced.⁶⁰ These CT recombination processes absolutely have a negative impact on the photovoltaic performance, consisting of open-circuit voltage (V_{oc}), short-circuit current (I_{sc}), and FF.

4 Methods for Photophysical Dynamics of Excitons and Charge Carriers

In this section, selected techniques for characterizing the dynamics of excitons and charge carriers in OSCs are summarized, with a focus on insights they offered into the photophysical processes of electronic states in organic optoelectronic materials. The purpose of this section is to emphasize the capabilities of the experimental methodologies that explore specific aspects related to photophysical phenomena, including exciton generation, exciton diffusion, charge separation, charge transport, and charge recombination. Moreover, a combination of these advanced characterization techniques allows us to further understand photophysical and electronic processes, enabling new insights into the development of new techniques.

Table 1 Comparison of various methods to measure exciton diffusion parameters.

Method	Measurement	Data analysis	Reference
Concentration-based quenching model	<ul style="list-style-type: none"> • Time-resolved PL decay • Concentration 	<ul style="list-style-type: none"> • Estimation of diffusion lifetime • PL decay fitting with hindered access model to estimate exciton diffusion coefficient • Calculation of exciton diffusion length 	73
TOF quenching model	<ul style="list-style-type: none"> • Time-resolved spectra • Film thickness • Complex index of refraction • Optical absorption spectra 	<ul style="list-style-type: none"> • Calculation of PL quenching efficiency • Estimation of exciton quenching fraction • Calculation of diffusion coefficient and diffusion lengths 	74
Monte Carlo simulation method	<ul style="list-style-type: none"> • Time-resolved PL decay • Film density 	<ul style="list-style-type: none"> • Calculation of quenching efficiency • PL decay fitting with Monte Carlo simulation model 	75–77
Photocurrent spectrum model	<ul style="list-style-type: none"> • The photocurrent of photovoltaic devices • Optical absorption 	<ul style="list-style-type: none"> • Estimation of exciton density distribution • Calculation of diffusion coefficient and diffusion lengths 	70, 78, and 79
Transient decays method	<ul style="list-style-type: none"> • Transient absorption spectra transient absorption decays • Transient decays at different temperatures 	<ul style="list-style-type: none"> • Analysis of triplet–triplet annihilation • Estimation of diffusion coefficient 	80
Exciton–exciton Annihilation	<ul style="list-style-type: none"> • Time-resolved PL at different excitation densities • Thickness and film density 	<ul style="list-style-type: none"> • PL decay fitting with an analytical model 	81 and 82
Förster resonance energy transfer theory	<ul style="list-style-type: none"> • Steady-state absorption, PL spectrum and PL quantum yield • Density and thickness of films • Index of refraction 	<ul style="list-style-type: none"> • Estimation of the distance between molecules • Calculation of the Förster radius and the diffusion coefficient 	67 and 72

4.1 Exciton Diffusion Parameters

In amorphous and polycrystalline organic semiconductor materials, the singlet exciton diffusion parameters (i.e., diffusion length and diffusion coefficient) are generally reported in the range of 5 to 20 nm and 3×10^{-4} to 5×10^{-3} cm² s⁻¹, respectively.^{63–70} It is still not thoroughly clear why exciton diffusion parameters are almost identical in a wide range of materials. What aspects have an influence on exciton diffusion parameters? How do these aspects correlate with the performance of photovoltaic devices? To figure out these answers, systematic investigations of exciton diffusion parameters are necessary for a series of materials with different chemical composition, morphology, and performance of solar cells.^{65,71,72} In the following, the available techniques for determining exciton diffusion parameters are summarized, and the strengths and weaknesses for each method are discussed. For the sake of providing a comprehensive comparison between these selected methods, Table 1 summarizes the measurement methods and data analysis of each technique to evaluate the exciton diffusion parameters. In the concentration-based quenching model,⁷³ the blended material/quencher films are spin-coated on the substrate. To investigate

the exciton diffusion, hindered-access-type quenching experiments are carried out whereby the PL decay of the material is monitored as a function of the addition of increasing concentrations of the quenchers (e.g., PCBM) for determining the diffusion-controlled quenching rate, k_q , which is then related to the exciton diffusion coefficient, D , and diffusion length, L_D . The time-of-flight quenching experiment⁷⁴ is performed by casting a series of material films of known and varying thickness (ca. 25 to 80 nm), on top of which a layer of the quencher is deposited (bilayer material/quencher films). In this configuration, the exciton lifetime varies with the film thickness since its natural decay via radiative and nonradiative processes competes with quenching at the quencher's interface, and the time needed for the exciton to arrive at the interface is related to the film thickness and the exciton diffusion parameters, D and L_D , respectively. The exciton quenching can also be analyzed by a Monte Carlo simulation,^{75–77} resulting in the estimation of exciton diffusion parameters. In the Monte Carlo simulation technique, the measured exciton diffusion lifetime in pristine materials is input into the Monte Carlo simulation where the diffusion coefficient is fitted to match the measured quenching efficiency at a given concentration of the quencher. In this technique, the exciton diffusion length is correlated to the distance an exciton is required to travel to reach a quencher molecule. Using photocurrent and optical absorption as a function of wavelength,^{70,78,79} the exciton diffusion parameters of the material can be estimated by several assumptions: (1) the current is limited by exciton diffusion to contacts; (2) the exciton diffusion is proportional to the space derivative of the exciton distribution; (3) the metal surfaces are perfect exciton quenchers so that the exciton densities at the surfaces are about zero. Transient decays⁸⁰ of triplet–triplet absorption of excited materials films are measured by the transient absorption of laser photolysis with a kinetic study containing a triplet–triplet annihilation in a wide temperature range (20 to 240 K). The rate constant of the triplet–triplet annihilation is analyzed by a diffusion model to obtain exciton diffusion parameters. As for the exciton–exciton annihilation method,^{81,82} time-resolved PL is monitored at variable excitation fluence to measure the decay of excitons because of the diffusion limited, collision, and annihilation. The exciton diffusion length is correlated to the exciton density at which most of generated excitons can be quenched via the exciton–exciton annihilation. In the bulk quenching methods, organic semiconductors are blended exciton quenchers to make homogeneous mixtures. Exciton quenching efficiency in blended films is detected as a function of quencher's concentration. The quenching process can be analyzed by a Monte Carlo simulation or the Stern–Volmer equation resulting in exciton diffusion parameters. For the Förster resonance energy transfer theory,^{67,72} the diffusion coefficient is calculated from the Förster radius and the distance between chromophores, and the exciton diffusion length is then evaluated using Eq. (3).

4.2 Charge Carrier Mobility

The molecular structure and the intermolecular interactions of organic and conjugated polymer semiconductors directly affect the charge transport characteristics. The charge carrier mobility of conjugated polymers depends on intrachain charge transport and interchain interactions, which are mainly mediated by thermally activated hopping.^{83,84} To enhance the performance of OSC devices, the efficient transport of separated charge carriers (holes and electrons) within the donor and acceptor materials is especially critical. In recent years, the alternative techniques, such as space-charge-limited current (SCLC),^{85–87} time-of-flight (TOF),^{88–90} carrier extraction by linearly increasing voltage (CELIV),^{91–93} photogenerated charges in CELIV (photo-CELIV),^{94–97} double injection (DI),^{98–100} field effect transistor,^{101–104} and impedance spectroscopy,^{105,106} are utilized to characterize the charge transport in organic semiconductors. However, not all of these characterization methods are applicable for a particular material. The selection of the method relies on the sample thickness, nature of the electrodes, and the energy levels of the materials. More detailed information of the SCLC, TOF, CELIV, photo-CELIV, and DI techniques are mainly discussed below.

The sample consisting of a thin organic semiconductor sandwiched between two electrodes is utilized to characterize the charge transport by a dark injection space-charge-limited current (DI-SCLC) method. In the DI-SCLC method, a step function voltage is applied to the injection contact of the sandwiched sample for both hole and electron mobility measurements. The typical

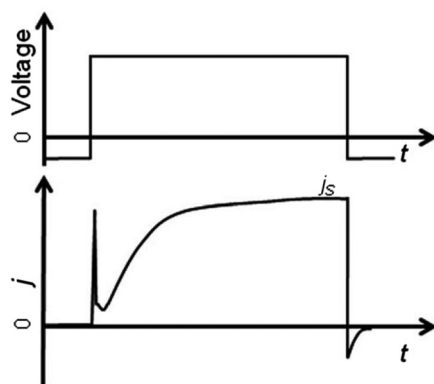


Fig. 4 A representative schematic for an ideal DI current transient. Reproduced with permission from Ref. 108. Copyright 2012 Wiley Periodicals, Inc.

observed current transient shows a peak at τ_{DI} (Fig. 4), which relates to the free carrier transit time t_{tr} as¹⁰⁷

$$\tau_{DI} = 0.787t_{tr}. \quad (4)$$

The t_{tr} obtained by Eq. (4) can be used to calculate the charge carrier mobility through Eq. (5):

$$\mu = \frac{v}{E} = \frac{d/t_{tr}}{V/d} = \frac{d^2}{Vt_{tr}}, \quad (5)$$

where V is the step function voltage and d is the sample thickness.

Because we can easily make thin films for organic molecules, the DI-SCLC method has been successfully utilized to measure the hole transport for small-molecule organic semiconductors such as 2,2',7,7'-tetrakis-(*N,N*-di-*p*-methoxyphenylamine)9,9'-spirobifluorene (spiro-MeOTAD),¹⁰⁹ 4,4'-bis[*N*-(1-naphthyl)-*N*-phenylamino]-biphenyl,¹¹⁰ and polyfluorene copolymers.^{111,112}

Furthermore, the trap-free SCLC method has been widely applied to characterize the charge transport and determine the charge carrier mobility in conjugated polymers for bulk heterojunction organic solar cells (BHJSCs). Blom et al.^{113–115} used this method to estimate hole and electron mobilities in the blends of poly(*p*-phenylene vinylene)s (PPV) and 6,6-phenyl C₆₁-butyric acid methyl ester (PCBM). Shrotriya et al.¹¹⁶ also utilized the SCLC technique to study the effect of the growth rate of phases in an active layer of BHJSC on the mobilities of its components, P3HT and PCBM. Although this technique has been widely used, a charge injection contact is still critical for SCLC. The SCLC methods cannot be utilized to detect hole mobility for organic semiconductors with very low HOMO levels or estimate electron mobilities for organic semiconductors with very high LUMO levels. For those specific materials, the TOF technique is one of the best choices.

The TOF method is very commonly used to determine charge carrier mobility in organic semiconductors. With regard to this measurement method, transparent/semitransparent electrode and a thicker film ($>1 \mu\text{m}$) of the organic semiconductor are requisite. In addition, the parameters, including dielectric relaxation time, sample thickness, and RC time constant, should be considered before measuring the charge carrier mobility using the TOF technique. In general, the dielectric relaxation time should be larger than the transit time, which is defined as the time for the photogenerated charges to relax back to the original state; sample thickness should be much larger than the inverse of the absorption coefficient; and the RC time constant should be significantly smaller than the transit time. The charge carrier mobility can be calculated as

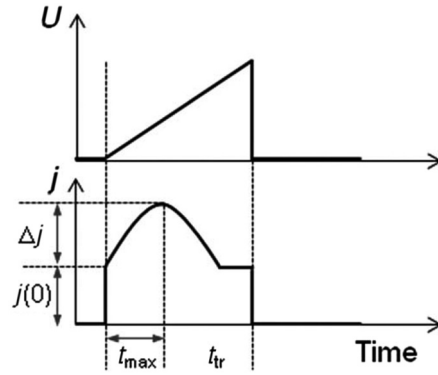


Fig. 5 A representative schematic for an ideal current transient obtained in CELIV for the applied voltage ramp. Reproduced with permission from Ref. 108. Copyright 2012 Wiley Periodicals, Inc.

$$\mu = \frac{d^2}{t_{tr} V}, \quad (6)$$

where V is the applied voltage, t_{tr} is the free carrier transit time, and d is the sample thickness.

As regards an advantage of the TOF technique, the mobility of both electron and hole charge carriers can be estimated from the same sample using this method. Moreover, many materials have been studied by the TOF method to obtain the electron and hole mobilities, including organic and organometallic molecules,^{117–119} conjugated polymers,^{120–122} and conjugated polymer networks.^{123,124}

CELIV has been recently used for the characterization of charge transport in organic semiconductors.^{91–93} The sample geometry and the required energy levels for the CELIV technique are similar to that for the TOF technique. However, in comparison to TOF measurements, the CELIV technique is applicable for thin films. The required thickness of spin-coated films is usually a few hundred nanometers for CELIV measurements. With regard to its other strength, the CELV technique allows us to measure charge carrier mobilities in materials with high bulk conductivity. Also, complete charge depletion from the prepared sample is not requisite. Accordingly, much weaker electric fields can be applied as compared with TOF measurements. The experimental setup utilized in CELIV measurements is similar to that employed in TOF technique, except that a linearly increasing voltage (ramp) pulse with slope, $A = U/t_{pulse}$ (where t_{pulse} is the duration of the ramp), is applied to the prepared sample.¹²⁵ Figure 5 shows a typical current transient obtained from a CELIV measurement. The increase of the initial step in the current is because of the capacitance of the prepared sample, given as

$$j(0) = \frac{\epsilon \epsilon_0 A}{d}, \quad (7)$$

where d is the film thickness.⁹¹ The increase in current after $j(0)$ is caused by the extraction of the dominant charge carrier present in the sample. The time required to reach the maximum in the extraction current (t_{max}) is used for the determination of the charge carrier mobility. The mobility is obtained from the measured current as

$$\mu = \frac{2d^2}{3At_{max}^2} \left[1 + 0.36 \frac{\Delta j}{j(0)} \right]^{-1}, \quad (8)$$

where A is the rate of increase of the applied voltage and Δj is the difference between the maximum current and $j(0)$. Equation (8) is valid when $\Delta j/j(0)$ is less than or close to one. In the case where $\Delta j/j(0) \leq 7$, numerical solutions to the equations describing the current transient yield a more precise expression for mobility given as¹²⁶

$$\mu = \frac{2d^2}{At_{\max}^2} [0.329e^{-0.180\Delta j/j(0)} + 0.005e^{0.253\Delta j/j(0)}]. \quad (9)$$

In organic semiconductors, the equilibrium charge carriers are commonly present by virtue of low-level doping or impurities. In the case of materials without these equilibrium charge carriers, sample under irradiation with a short laser pulse can be used to collect photogenerated charge carriers, which can then be extracted from the film after a certain delay. This modified technique is typically referred to as photo-CELIV and the charge carrier mobility can be estimated by utilizing equations used for CELIV measurements.¹²⁷ The photo-CELIV technique has also been applied to determine the mobilities in the active layers of BHJSC. In the photo-CELIV technique, long photo pulse and constant illumination could also be utilized. For photo-CELIV, the distribution of the photogenerated charge carriers and their recombination effects have also been studied. These effects may show serious errors under certain conditions. More experimental application associated with the photo-CELIV technique can be found in Refs. 94, 96, and 97. As a result of the diverse strengths of the CELIV and photo-CELIV techniques, these techniques are being increasingly utilized for the measurement of charge carrier mobilities in donor–acceptor blends.^{128–130}

The DI transient technique can be used for samples with injecting contacts, whereas the TOF technique cannot be applied. The DI technique does not need a laser pulse for the photoexcitation of organic materials. Also, through the selected electrodes, both the electrons and holes are injected into samples. The effect of both electric field and temperature on charge carrier mobility can be detected by utilizing the DI technique. The experimental setup used for DI is analogous to that utilized in TOF. In this technique, a step function voltage is applied to the samples in the forward bias, injecting both electrons and holes in the sample, and then the current transient is obtained from the oscilloscope (Fig. 6). The determination of charge carrier mobility depends on the relation between τ_{σ} and t_{tr} . For the samples with high conductivity, the saturated DI current can be calculated by Eq. (10) when $\tau_{\sigma} \ll t_{tr}$:

$$J_s = \frac{8V_{\epsilon\epsilon_0}}{9d} \sqrt{\frac{\beta_L}{\beta} \frac{1}{\tau_{\sigma} t_a}}, \quad (10)$$

where d is the sample thickness, β is the bimolecular recombination coefficient, β_L is the Langevin recombination coefficient, and t_a is the ambipolar carrier transit time.

The ambipolar charge carrier mobility can be calculated using t_a ; however, it might be ambiguous in the current transient. Thus, a derivative of the current transient is plotted, from which the obtained inflexion point (t_m) is used to estimate the ambipolar charge carrier mobility (μ_a)

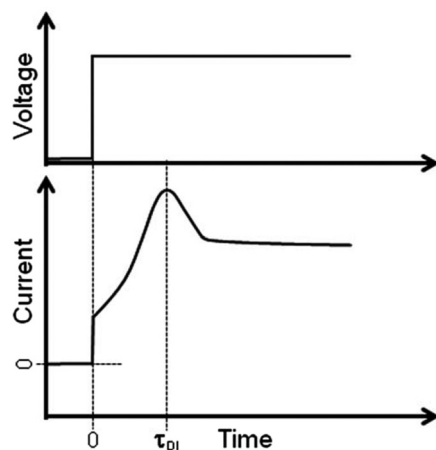


Fig. 6 A representative schematic for an ideal current transient obtained in DI for the applied step voltage. Reproduced with permission from Ref. 108. Copyright 2012 Wiley Periodicals, Inc.

$$t_a = \frac{6t_m}{5} = \frac{d^2}{V\mu_a}. \quad (11)$$

For low conductivity samples, the saturated DI current is expressed below when $\tau_\sigma \gg t_{tr}$ and when the recombination is Langevin type¹⁰⁷

$$J_s = \frac{9}{8} \varepsilon \varepsilon_0 (\mu_e + \mu_h) \frac{V^2}{d^3}, \quad (12)$$

where ε is the dielectric permittivity, ε_0 is the relative permittivity, μ_e (μ_h) is the electron (hole) mobility, V is an external applied voltage, and d is the sample thickness. In addition, the recombination coefficient of bimolecules can also be estimated by the DI transient technique. This technique has been utilized to investigate the ambipolar charge carrier mobility and the charge carrier recombination in a variety of conjugated polymer-PCBM blends.^{98,99,131-133}

4.3 Time-Resolved Spectroscopy

The charge carrier dynamics in OSC devices are investigated utilizing time-resolved spectroscopy, such as pump-probe techniques,¹³⁴⁻¹³⁷ time-resolved microwave conductivity (TRMC),¹³⁸⁻¹⁴⁰ time-resolved vibrational spectroscopy,^{141,142} time-resolved two-photon,^{142,143} and x-ray photoemission.^{144,145} Here, we mainly focus on the discussion of pump-probe technique and TRMC techniques.

Time-resolved pump-probe spectroscopy is a powerful technique for the characterization of excited states and the charge carrier dynamics of various materials, providing a complete photo-physical picture. For the basic configuration of pump-probe techniques, two pulsed beams (a pump and a probe) are incident on a sample, and the time delay between the pulses is controlled with a delay line. The transmission or reflection of the probe beam is monitored as a function of time delay with respect to the pump beam. The typical pump-probe experiment is shown in Fig. 7. An excited state of the sample is generated by absorbing a first energetic pump pulse, while a second delayed and weaker pulse tracks the pump-induced changes in the optical response. The probe can be obtained either by attenuating the pump pulse using a beam splitter (degenerate pump-probe) or generating a pulse with a different color (nondegenerate pump-probe). The pulse duration and bandwidth are significant features of the experiment. The temporal resolution of the experiment is only limited by the duration of pump and probe pulses, which is <100 fs in the commercial femtosecond systems. As for the bandwidth, the pump pulse should not be too broad to enable selective excitation of an optical transition. Moreover, the probe pulse, which is ideally a transform-limited, δ -function white light pulse, should be as short as possible (for simultaneously measuring transmission changes at many different wavelengths).¹⁴⁶

In recent years, time-resolved pump-probe spectroscopy has achieved considerable development in terms of temporal resolution and pulse frequency bandwidth, which allows us to monitor a wider range of transitions and their interplay on the earliest photophysical processes. Nonetheless, to explore the effect of local environment on the photophysical processes and the external factors in optoelectronic devices, the interactions between excited states need to be further investigated to build a more complete picture. An advanced technique with both

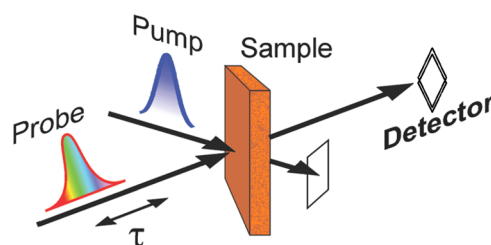


Fig. 7 Scheme of a pump-probe experiment. Reproduced with permission from Ref. 147. Copyright 2007 The Royal Society of Chemistry.

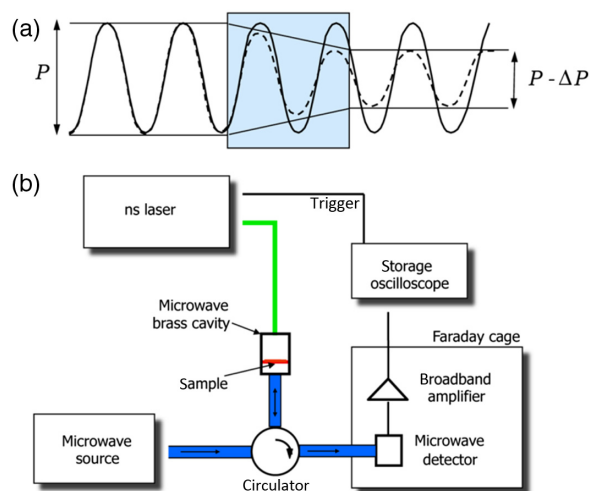


Fig. 8 (a) Attenuation of microwaves propagating through a weakly conducting medium and (b) schematic representation of the time-resolved microwave photoconductance setup. Reproduced with permission from Ref. 140. Copyright 2013 American Chemical Society.

100 fs resolution and diffraction limited spatial resolution, pump–probe spectroscopy combined with a confocal microscope was then developed to study the influence of morphology. Notably, this new technique has been favorable for imaging polaron-pairs that delocalize over two polymer chains. In the blended films of PFO/PMMA, the submicron size regions were confirmed to be fully isolated PFO chains, exhibiting highly impressive interesting photonic properties.¹⁴⁶ In addition, the electric field-assisted transient absorption spectroscopy technique,¹⁴⁸ which can probe the difference in the transmission of the probe beam through the sample with and without an applied electric field, is utilized to readily discriminate the populations of the neutral and charged states.

TRMC is an alternative method for performing fast photoconductivity measurements to characterize the charge carrier mobility and the charge carrier generation efficiency. In contrast with TOF measurements, this technique is an electrodeless technique, avoiding the requirement to use Ohmic electrodes and therefore removing the effects owing to active layer–electrode interfaces. In the TRMC experiment, the fabricated sample is excited by either an optical pulse or a highly energetic electron beam, and the transmission or reflection of microwave probe pulse is detected. According to the decrease of amplitude and/or a change in the phase of the electric field of a microwave probe with nanosecond time resolution, this noncontact technique allows one to probe real and imaginary parts of conductivity. Savenije et al.¹³⁸ first applied the photo-induced TRMC technique to measure the effect of the blended ratio between the polymer (a polyphenylene-vinylene derivative) and the PCBM. In general, the microwave photoconductance setup includes four vital portions: (1) a stable microwave source; (2) a pulsed, tunable photoexcitation source; (3) a microwave cell loaded with the sample of interest; and (4) a sensitive detection and data acquisition system. TRMC experiments can be executed in the transmission mode, as shown in Fig. 8(a). Nonetheless, all present experiments have been implemented in the reflection mode, thus requiring the incorporation of a microwave circulator, separating the reflected part from the incident microwaves as shown in Fig. 8(b). The TRMC technique has offered valuable insights into the nanosecond–microsecond charge carrier dynamics in polymer-based BHJs.^{139,140}

4.4 Scanning Probe Microscopy

The scanning probe microscopy (SPM) method has been used to measure current flows, charge distribution, resistance, capacitance, electrostatic forces, charge distribution, surface potential, PL, and so on. The correlation between surface morphology and charge transport properties at microscopic scales in organic semiconductors has been carried out using near-field scanning optical microscopy (NSOM), conductive AFM (c-AFM), Kelvin probe scanning microscopy, etc. The analysis of experimental results has provided the photophysical information related

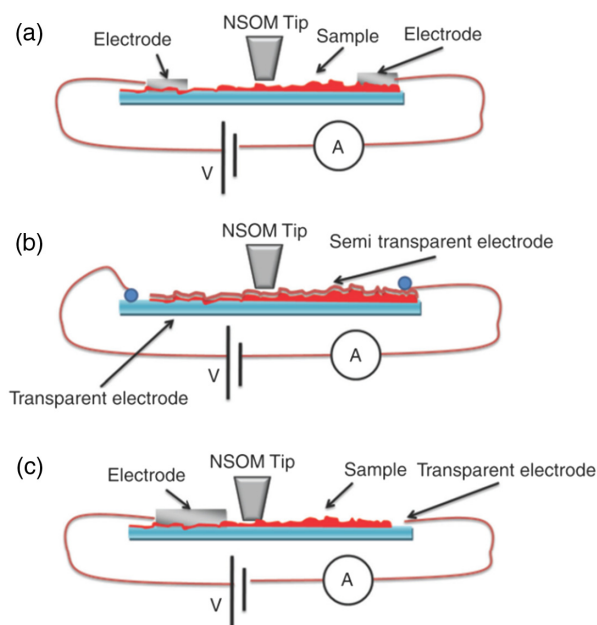


Fig. 9 Different models of p-NSOM. (a) Scanning region lies in between lateral electrodes. (b) Scanning is carried out on a semitransparent electrode. (c) Scanning region lies in the vicinity of the electrode. In (b) and (c) the bottom electrode is generally a transparent electrode such as indium tin oxide. Typically, a voltage is applied in geometry (a) and (b). A voltage source is generally not necessary in configuration (c). In each case, critical optoelectronic features can be extracted in addition to the topology and photocurrent images. A combination of these images is very effective in arriving at a complete visualization and functionality of the sample. Reproduced with permission from Ref. 157. Copyright 2013 Walter de Gruyter GmbH.

to charge generation,^{149–151} charge transport properties,^{152,153} and the kinetics of charge trapping and detrapping.^{46,47} More detailed information of SPM concerning investigations of the photo-induced carrier dynamics can be found in Refs. 138 and 139. In this section, the common methods related to SPM techniques will be further discussed.

NSOM has been successfully utilized to probe and characterize optical properties of single molecules and nanomaterials.^{154–156} This technique enables simultaneous assessment of surface topology and optical absorption, PL, and/or photoconductive properties. The NSOM technique can be carried out on conventional optical microscope platforms, making it much more versatile for different operation modes, including illumination transmission, collection, illumination collection, reflection, and reflection collection operated under either the sample or the detector in the near-field regime. Importantly, the NSOM technique is also applied to investigate photoconductivity or the generation of current under illumination. Photoconductivity is a significant property of active semiconductor materials in solar cells and photodetectors. In the photoconductive NSOM (p-NSOM) mode, the working device consists of a photoconductive material for current generation under illumination. Hence, the p-NSOM mode can be realized by employing the illumination, the illumination collection, or the reflection modes of p-NSOM. As shown in Fig. 9, the p-NSOM is generally classified into three categories: (a) lateral electrode, (b) transparent electrode geometry, and (c) electrode periphery geometry. Each mode of p-NSOM techniques is suitable for the specified device and can offer simultaneous information related to topography, photocurrent, fluorescence, and transmission in many cases.

The standard c-AFM employs an inverted confocal microscope to illuminate the sample from the transparent electrode, and the c-AFM image is performed by scanning a conductive tip across a sample at a fixed voltage, as shown in Fig. 10.¹⁵⁷ This technique can be applied to simultaneously collect a current map and the topology in various organic materials. The charge carrier dynamics in OSCs can also be further explored by c-AFM.¹⁵⁸ In terms of the quality of images, the c-AFM without using the near-field can produce a high-resolution image similar to the result conducted using an AFM cantilever. Pingree et al.¹⁵⁹ utilized this method to examine the

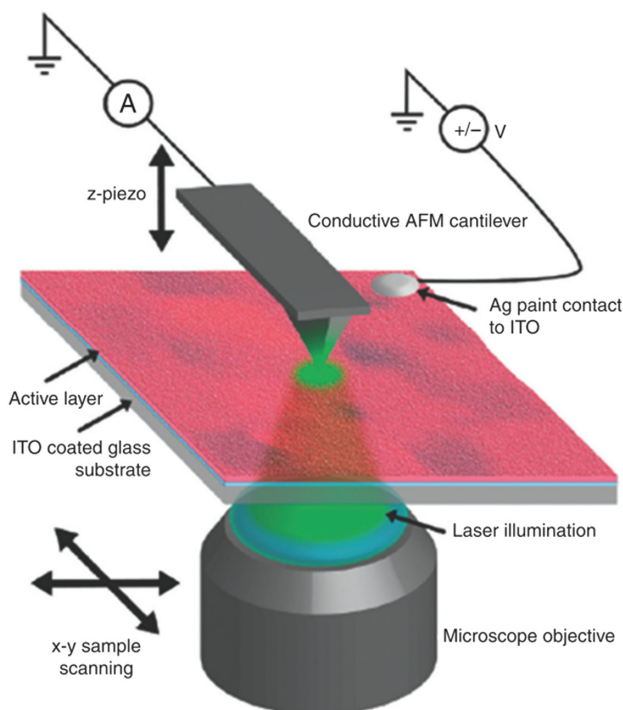


Fig. 10 The configuration of C-AFM. Illumination of light created photogenerated charge carriers which alter the local conductivity. A c-AFM tip can be used to map photoconductive regions. Reproduced with permission from Ref. 157. Copyright 2013 Walter de Gruyter GmbH.

evolution of morphology and spatial variations of the photocurrent across various domains in P3HT:PCBM blends of OSCs under thermal annealing. In addition, they found that the regions of highest dark hole currents, highest dark electron currents, and highest photocurrents after annealing were associated with different regions of the nanostructured films. Dante et al.¹⁶⁰ simultaneously studied changes of the film morphology and the charge transport for P3HT:PCBM blended films upon thermal annealing. Moerman et al.¹⁶¹ reported that the lateral spatial resolution of c-AFM technique is down to 5 nm, but quantitative analysis of the charge transport is complicated by the uncertainty in the tip-sample contact area.^{162,163} To remedy this uncertainty, the mechanical and electrical properties of the active materials (e.g., of P3HT films) were simultaneously mapped out utilizing c-AFM.

Kelvin probe force microscopy (KPFM), also known as Kelvin probe microscopy, is another scanning probe technique based on dynamic force microscopy mapping both film surface topology and the electric potential with high spatial and electrical resolution. Kelvin¹⁶⁴ first introduced the KPFM technique, which is a combination of the macroscopic Kelvin probe technique and the AFM technique. The standard KPFM method measures the electrostatic interaction between the sample and a vibrating conductive probe mounted at the edge of a cantilever.^{165,166} The electrostatic force is produced by the alignment of Fermi levels between the probe and the sample during the measurement process. The KPFM technique is noncontact, which can be utilized to determine the work function and surface potential distribution even in poorly conducting films.^{166,167} This technique employed in working devices can probe photo-physical processes, such as charge photogeneration and detrapping, under illumination.¹⁶⁸ Palermo et al.¹⁶⁹ utilized this KPFM technique to study the charging and discharging dynamics of donor and acceptor domains in P3HT-based BHJSCs under the pulsed illumination. However, the time resolution of this technique is on the order of milliseconds; thus, faster processes cannot be detected. Recent developments consisting of multifrequency band excitation KPFM and 3D-KPFM techniques have further improved tip-sample deconvolution and bulk sensitivity.^{170,171}

4.5 Optical Absorption and Photoluminescence Imaging

The absorption and PL microscopies of organic semiconductors have been widely used to study domains and interfaces in donor–acceptor blends,¹⁷² evaluate exciton diffusion processes,^{173,174} probe the nature of exciton states depending on the molecular order in crystalline films,¹⁷⁵ examine the exciton delocalization,¹⁷⁶ and so forth. Irkhin and Biaggio¹⁷³ studied the exciton diffusion in rubrene single crystals using localized photoexcitation and spatially resolved detection of the excitonic luminescence. They utilized this technique to directly observe exciton diffusion and exciton mobility anisotropy in molecular crystals and determined a triplet diffusion length of $4.0 \pm 0.4 \mu\text{m}$ along the *b*-axis of rubrene single crystals. This imaging technique enables the investigation of exciton diffusion under different experimental conditions and in different materials, thus extending the exploration of exciton diffusion phenomena and exciton transport processes in organic molecular crystals. Deotare et al.¹⁷⁴ reported direct nanoscale imaging of the charge transport in a donor–acceptor blend of m-MTDATA:3TPYMB, which proved that the bound electron–hole pairs moved geminately over distances of 5 to 10 nm as a result of energetic disorder and diffusion to lower energy sites. The variation in electron–hole spacing during the diffusion was observed by the shape of the magnetic field dependence as a function of temperature. The results revealed that the electron–hole pair of charge carrier states underwent a stretching transport mechanism such as an “inchworm” motion. By virtue of the rapid conversion from excitons to CT states for donor and acceptor blends, it is possible that the diffusion distance of CT states in many organic devices exceed the initial exciton, indicating the potential impact of charge carrier transport on device performance. Sharifzadeh et al.¹⁷⁶ combined the spatially resolved polarization-dependent linear optical absorption measurement with *ab initio* density functional theory as well as many-body perturbation theory to explore the relationship between optical absorption properties and solid-state structure for solid-state organic 6,13-bis(triisopropylsilylethynyl)-pentacene. They found that the lowest energy exciton in the bulk is delocalized and the distribution of the exciton is over ≈ 3 nm (over three molecules). Regarding the properties of singlet fission, singlet–triplet energy splitting, the degree of delocalization, and charge-transfer character of the singlet exciton are highly tunable with the control of π -orbital stacking, so solid-state structures can be tailored for the optimization of singlet fission with appropriate functionalization or growth conditions. Recently, Rawat et al.¹⁷⁵ reported that metal-free phthalocyanine crystalline films were characterized by spatially, temporally, and polarization-resolved PL/linear dichroism microscopy. The experimental results showed the temperature-induced switching between localized and delocalized excited states was related to a change in the tilt of the long molecular axis.

5 Conclusion and Future Perspectives

In this review, we systematically discussed the recent progress in the understanding of photophysical mechanisms and characterization in organic photovoltaic devices. The contribution of this review is first intended to discuss the exciton transfer process. The two main mechanisms, Förster energy transfer and Dexter energy transfer in OSCs, are emphatically introduced. In the following section, the mechanisms of charge carrier transport, including charge carrier generation as well as charge carrier trapping recombination, are further discussed. Until now, several methodologies related to photophysical methods have been reported for characterization of the photophysical dynamics of excitons and charge carriers. The common techniques such as concentration-based quenching model, TOF quenching model, Monte Carlo simulation method, and so forth have been utilized to identify the exciton diffusion length parameters. Time-resolved spectroscopy, SPM, optical absorption, and PL imaging techniques have been applied to investigate the charge carrier transport and estimate charge carrier mobilities.

The primary motivation in the area of OSCs largely stems from the potential applications of organic semiconductor materials. However, many interesting phenomena related to investigations of photophysical processes using advanced characterization techniques still remain unclear and need to be further explored. More comprehensive research is compulsory in all aspects of the field, including theoretical descriptions of exciton energy transfer and charge carrier transport, experimental discovery and validation, as well as systematic materials design. Theoretical

models of exciton and charge generation require they be combined with the spin-dependent dynamics, delocalization, and microscopic characteristics of the materials. The qualitative and quantitative determination of exciton and charge generation need much deeper investigations to further enhance the efficiency and stability of organic optoelectronic devices, including but not limited to solar cells, transistors, photodetectors, image sensors, and light-emitting diodes.

Disclosures

The authors declare that they have no conflicts of interest to this work.

Acknowledgments

The authors acknowledge financial support from the Strategic Research at City University of Hong Kong (Grant Nos. 7004928, 6000595, 7200525, and 9680208) and the SZSTI grant of Shenzhen Municipality (Grant No. R-IND12301).

References

1. S. R. Forrest, "The path to ubiquitous and low-cost organic electronic appliances on plastic," *Nature* **428**, 911–918 (2004).
2. C. J. Brabec, "Organic photovoltaics: technology and market," *Sol. Energy Mater. Sol. Cells* **83**, 273–292 (2004).
3. G. Li, R. Zhu, and Y. Yang, "Polymer solar cells," *Nat. Photonics* **6**, 153–161 (2012).
4. C. W. Tang, "Two-layer organic photovoltaic cell," *Appl. Phys. Lett.* **48**, 183–185 (1986).
5. N. S. Sariciftci et al. "Photoinduced electron transfer from a conducting polymer to buckminsterfullerene," *Science* **258**, 1474–1476 (1992).
6. B. Kraabel et al., "Ultrafast photoinduced electron transfer in conducting polymer—buckminsterfullerene composites," *Chem. Phys. Lett.* **213**, 389–394 (1993).
7. N. Sariciftci et al., "Semiconducting polymers (as donors) and buckminsterfullerene (as acceptor): photoinduced electron transfer and heterojunction devices," *Synth. Met.* **59**, 333–352 (1993).
8. M. Hiramoto, H. Fujiwara, and M. Yokoyama, "p-I-n like behavior in three-layered organic solar cells having a co-deposited interlayer of pigments," *J. Appl. Phys.* **72**, 3781–3787 (1992).
9. J. Halls et al., "Efficient photodiodes from interpenetrating polymer networks," *Nature* **376**, 498–500 (1995).
10. G. Yu et al., "Polymer photovoltaic cells: enhanced efficiencies via a network of internal donor–acceptor heterojunctions," *Science* **270**, 1789–1791 (1995).
11. W. Zhao et al., "Environmentally friendly solvent-processed organic solar cells that are highly efficient and adaptable for the blade-coating method," *Adv. Mater.* **30**, 1704837 (2018).
12. B. A. Gregg, "Excitonic solar cells," *J. Phys. Chem. B* **107**, 4688–4698 (2003).
13. W. E. Shepherd et al., "Energy transfer and exciplex formation and their impact on exciton and charge carrier dynamics in organic films," *J. Phys. Chem. Lett.* **2**, 362–366 (2011).
14. J.-L. Brédas et al., "Charge-transfer and energy-transfer processes in π -conjugated oligomers and polymers: a molecular picture," *Chem. Rev.* **104**, 4971–5004 (2004).
15. Y. Zhao and W. Liang, "Charge transfer in organic molecules for solar cells: theoretical perspective," *Chem. Soc. Rev.* **41**, 1075–1087 (2012).
16. O. Ostroverkhova, "Organic optoelectronic materials: mechanisms and applications," *Chem. Rev.* **116**, 13279–13412 (2016).
17. S. M. Menke and R. J. Holmes, "Exciton diffusion in organic photovoltaic cells," *Energy Environ. Sci.* **7**, 499–512 (2014).
18. D. L. Dexter, "A theory of sensitized luminescence in solids," *J. Chem. Phys.* **21**, 836–850 (1953).
19. D. Dexter, R. Knox, and T. Förster, "The radiationless transfer of energy of electronic excitation between impurity molecules in crystals," *Phys. Status Solidi B* **34**, K159–K162 (1969).

20. G. D. Scholes, "Long-range resonance energy transfer in molecular systems," *Annu. Rev. Phys. Chem.* **54**, 57–87 (2003).
21. N. J. Turro, *Modern Molecular Photochemistry*, University Science Books, Mill Valley, California (1991).
22. N. J. Turro, V. Ramamurthy, and J. C. Scaiano, *Principles of Molecular Photochemistry: An Introduction*, University Science Books, Sausalito, California (2009).
23. R. Koeppe and N. Sariciftci, "Photoinduced charge and energy transfer involving fullerene derivatives," *Photochem. Photobiol. Sci.* **5**, 1122–1131 (2006).
24. J. Kalinowski et al., "Triplet energy exchange between fluorescent and phosphorescent organic molecules in a solid state matrix," *Chem. Phys.* **297**, 39–48 (2004).
25. Y. Kawamura et al., "Intermolecular interaction and a concentration-quenching mechanism of phosphorescent Ir (III) complexes in a solid film," *Phys. Rev. Lett.* **96**, 017404 (2006).
26. O. V. Mikhnenko et al., "Trap-limited exciton diffusion in organic semiconductors," *Adv. Mater.* **26**, 1912–1917 (2014).
27. D. Markov et al., "Simultaneous enhancement of charge transport and exciton diffusion in poly (p-phenylene vinylene) derivatives," *Phys. Rev. B* **72**, 045217 (2005).
28. J. Yang et al., "Simultaneous enhancement of charge transport and exciton diffusion in single-crystal-like organic semiconductors," *Appl. Phys. Lett.* **100**, 103305 (2012).
29. J. Lee et al., "Charge transfer state versus hot exciton dissociation in polymer–fullerene blended solar cells," *J. Am. Chem. Soc.* **132**, 11878–11880 (2010).
30. F. Gao and O. Inganäs, "Charge generation in polymer–fullerene bulk-heterojunction solar cells," *Phys. Chem. Chem. Phys.* **16**, 20291–20304 (2014).
31. H. Ohkita et al., "Charge carrier formation in polythiophene/fullerene blend films studied by transient absorption spectroscopy," *J. Am. Chem. Soc.* **130**, 3030–3042 (2008).
32. T. Virgili et al., "Ultrafast intrachain photoexcitation of polymeric semiconductors," *Phys. Rev. Lett.* **94**, 117402 (2005).
33. T. M. Clarke et al., "Free energy control of charge photogeneration in polythiophene/fullerene solar cells: the influence of thermal annealing on P3HT/PCBM blends," *Adv. Funct. Mater.* **18**, 4029–4035 (2008).
34. A. A. Bakulin et al., "Charge-transfer state dynamics following hole and electron transfer in organic photovoltaic devices," *J. Phys. Chem. Lett.* **4**, 209–215 (2012).
35. S. Albrecht et al., "On the field dependence of free charge carrier generation and recombination in blends of PCPDTBT/PC₇₀BM: influence of solvent additives," *J. Phys. Chem. Lett.* **3**, 640–645 (2012).
36. K. Vandewal et al., "Efficient charge generation by relaxed charge-transfer states at organic interfaces," *Nat. Mater.* **13**, 63–68 (2014).
37. I. A. Howard et al., "Effect of morphology on ultrafast free carrier generation in polythiophene:fullerene organic solar cells," *J. Am. Chem. Soc.* **132**, 14866–14876 (2010).
38. T. Wang et al., "A multidimensional view of charge transfer excitons at organic donor–acceptor interfaces," *J. Am. Chem. Soc.* **139**, 4098–4106 (2017).
39. S. Athanasopoulos et al., "Efficient charge separation of cold charge-transfer states in organic solar cells through incoherent hopping," *J. Phys. Chem. Lett.* **8**, 2093–2098 (2017).
40. H. Bässler and A. Köhler, "'Hot or cold: how do charge transfer states at the donor–acceptor interface of an organic solar cell dissociate?'" *Phys. Chem. Chem. Phys.* **17**, 28451–28462 (2015).
41. R. A. Street, "Hydrogenated amorphous silicon cambridge solid state science series," R. W. Cahn, E. W. Davis, and I. M. Ward, Eds., Cambridge University Press (1991).
42. A. Salleo, "Electronic traps in organic semiconductors," in *Organic Electronics: Emerging Concepts and Technologies*, F. Cicoira and C. Santato, Eds., pp. 341–380, Wiley-VCH, Weinheim, Germany (2013).
43. J. J. Benson-Smith et al., "Formation of a ground-state charge-transfer complex in polyfluorene/[6,6]-phenyl-C₆₁ butyric acid methyl ester (PCBM) blend films and its role in the function of polymer/PCBM solar cells," *Adv. Funct. Mater.* **17**, 451–457 (2007).
44. L. Goris et al., "Observation of the subgap optical absorption in polymer–fullerene blend solar cells," *Appl. Phys. Lett.* **88**, 052113 (2006).

45. K. Vandewal et al., "Highly sensitive spectroscopic characterization of inorganic and organic heterojunctions for solar cells," *Eur. Phys. J. Appl. Phys.* **36**, 281–283 (2006).
46. M. Jaquith, E. M. Muller, and J. A. Marohn, "Time-resolved electric force microscopy of charge trapping in polycrystalline pentacene," *J. Phys. Chem. B* **111**, 7711–7714 (2007).
47. M. J. Jaquith, J. E. Anthony, and J. A. Marohn, "Long-lived charge traps in functionalized pentacene and anthradithiophene studied by time-resolved electric force microscopy," *J. Mater. Chem.* **19**, 6116–6123 (2009).
48. J. L. Luria et al., "Spectroscopic characterization of charged defects in polycrystalline pentacene by time- and wavelength-resolved electric force microscopy," *Adv. Mater.* **23**, 624–628 (2011).
49. T. N. Ng, W. R. Silveira, and J. A. Marohn, "Dependence of charge injection on temperature, electric field, and energetic disorder in an organic semiconductor," *Phys. Rev. Lett.* **98**, 066101 (2007).
50. J. D. Slinker et al., "Direct measurement of the electric-field distribution in a light-emitting electrochemical cell," *Nat. Mater.* **6**, 894–899 (2007).
51. C. Renaud and T.-P. Nguyen, "Identification of the nature of trapping centers in polyspirobifluorene based diodes by using electrical characterization," *J. Appl. Phys.* **107**, 124505 (2010).
52. I. Thurzo, H. Méndez, and D. Zahn, "Analysis of charge transient spectroscopy data originating from Gaussian densities of electron states in organics," *Phys. Status Solidi A* **202**, 1994–2007 (2005).
53. W. Weise et al., "Trap concentration dependence of thermally stimulated currents in small molecule organic materials," *Phys. Rev. B* **72**, 045202 (2005).
54. P. Stallinga and H. L. Gomes, "Modeling electrical characteristics of thin-film field-effect transistors: II: effects of traps and impurities," *Synth. Met.* **156**, 1316–1326 (2006).
55. M. Pranaitis et al., "Determination of the charge trap energy distribution in conjugated polymer MDMO-PPV," *Semicond. Sci. Technol.* **26**, 085021 (2011).
56. O. Gaudin et al., "Determination of traps in poly (p-phenylene vinylene) light emitting diodes by charge-based deep level transient spectroscopy," *J. Appl. Phys.* **90**, 4196–4204 (2001).
57. T. Nguyen et al., "Determination of localized trap parameters in organic semiconductors using charge based deep level transient spectroscopy (Q-DLTS)," *Eur. Phys. J. Appl. Phys.* **27**, 219–222 (2004).
58. A. C. Morteani et al., "Exciton regeneration at polymeric semiconductor heterojunctions," *Phys. Rev. Lett.* **92**, 247402 (2004).
59. D. Veldman, S. C. Meskers, and R. A. Janssen, "The energy of charge-transfer states in electron donor–acceptor blends: insight into the energy losses in organic solar cells," *Adv. Funct. Mater.* **19**, 1939–1948 (2009).
60. C. Deibel, T. Strobel, and V. Dyakonov, "Role of the charge transfer state in organic donor–acceptor solar cells," *Adv. Mater.* **22**, 4097–4111 (2010).
61. T. Ford et al., "Direct observation of intersystem crossing in charge-pair states in polyfluorene polymer blends," *Chem. Phys. Lett.* **454**, 237–241 (2008).
62. T. Offermans et al., "Exciplex dynamics in a blend of π -conjugated polymers with electron donating and accepting properties: MDMO-PPV and PCNEPV," *Phys. Rev. B* **72**, 045213 (2005).
63. W. A. Luhman and R. J. Holmes, "Investigation of energy transfer in organic photovoltaic cells and impact on exciton diffusion length measurements," *Adv. Funct. Mater.* **21**, 764–771 (2011).
64. P. Peumans, A. Yakimov, and S. R. Forrest, "Small molecular weight organic thin-film photodetectors and solar cells," *J. Appl. Phys.* **93**, 3693–3723 (2003).
65. Y. Terao, H. Sasabe, and C. Adachi, "Correlation of hole mobility, exciton diffusion length, and solar cell characteristics in phthalocyanine/fullerene organic solar cells," *Appl. Phys. Lett.* **90**, 103515 (2007).
66. O. Mikhnenko et al., "Temperature dependence of exciton diffusion in conjugated polymers," *J. Phys. Chem. B* **112**, 11601–11604 (2008).

67. R. R. Lunt et al., "Exciton diffusion lengths of organic semiconductor thin films measured by spectrally resolved photoluminescence quenching," *J. Appl. Phys.* **105**, 053711 (2009).
68. D. Markov and P. Blom, "Anisotropy of exciton migration in poly (p-phenylene vinylene)," *Phys. Rev. B* **74**, 085206 (2006).
69. H. Wang et al., "Exciton diffusion and charge transfer dynamics in nano phase-separated P3HT/PCBM blend films," *Nanoscale* **3**, 2280–2285 (2011).
70. J. J. Halls et al., "Exciton diffusion and dissociation in a poly (p-phenylenevinylene)/C₆₀ heterojunction photovoltaic cell," *Appl. Phys. Lett.* **68**, 3120–3122 (1996).
71. L. D. Siebbeles, A. Huijser, and T. J. Savenije, "Effects of molecular organization on exciton diffusion in thin films of bioinspired light-harvesting molecules," *J. Mater. Chem.* **19**, 6067–6072 (2009).
72. R. R. Lunt, J. B. Benziger, and S. R. Forrest, "Relationship between crystalline order and exciton diffusion length in molecular organic semiconductors," *Adv. Mater.* **22**, 1233–1236 (2010).
73. H.-Y. Hsu et al., "Triplet exciton diffusion in platinum polyyne films," *J. Phys. Chem. C* **118**, 24282–24289 (2014).
74. M. Theander et al., "Photoluminescence quenching at a polythiophene/C₆₀ heterojunction," *Phys. Rev. B* **61**, 12957–12963 (2000).
75. J. E. Kroeze et al., "Triplet exciton diffusion and delayed interfacial charge separation in a TiO₂/PdTPPC bilayer: Monte Carlo simulations," *Sol. Energy Mater. Sol. Cells* **85**, 189–203 (2005).
76. O. V. Mikhnenko et al., "Effect of thermal annealing on exciton diffusion in a diketopyrrolopyrrole derivative," *Phys. Chem. Chem. Phys.* **14**, 14196–14201 (2012).
77. O. V. Mikhnenko et al., "Exciton diffusion length in narrow bandgap polymers," *Energy Environ. Sci.* **5**, 6960–6965 (2012).
78. M. Black, C. Chavez, and E. Brosha, "Exciton diffusion length of tris (dibenzoylmethane) mono (phenanthroline) europium (III) measured by photocurrent and absorption as a function of wavelength," *Org. Electron.* **8**, 601–605 (2007).
79. D. Qin et al., "Measuring the exciton diffusion length of C₆₀ in organic planar heterojunction solar cells," *Phys. Status Solidi A* **208**, 1967–1971 (2011).
80. A. Tsuchida et al., "Triplet energy migration in poly (4-methacryloylbenzophenone-co-methyl methacrylate) films: temperature dependence and chromophore concentration dependence," *Macromolecules* **29**, 1589–1594 (1996).
81. S. Cook et al., "Estimate of singlet diffusion lengths in PCBM films by time-resolved emission studies," *Chem. Phys. Lett.* **478**, 33–36 (2009).
82. A. Lewis et al., "Singlet exciton diffusion in MEH-PPV films studied by exciton–exciton annihilation," *Org. Electron.* **7**, 452–456 (2006).
83. C. J. Brabec, N. S. Sariciftci, and J. C. Hummelen, "Plastic solar cells," *Adv. Funct. Mater.* **11**, 15–26 (2001).
84. G. Horowitz, "Organic field-effect transistors," *Adv. Mater.* **10**, 365–377 (1998).
85. S. Tse, S. Tsang, and S. So, "Polymeric conducting anode for small organic transporting molecules in dark injection experiments," *J. Appl. Phys.* **100**, 063708 (2006).
86. C. Y. Liu and S. A. Chen, "Charge mobility and charge traps in conjugated polymers," *Macromol. Rapid Commun.* **28**, 1743–1760 (2007).
87. S. Tsang, S. So, and J. Xu, "Application of admittance spectroscopy to evaluate carrier mobility in organic charge transport materials," *J. Appl. Phys.* **99**, 013706 (2006).
88. K. Tsung and S. So, "Carrier trapping and scattering in amorphous organic hole transporter," *Appl. Phys. Lett.* **92**, 103315 (2008).
89. F. Laquai et al., "Nondispersive hole transport in carbazole- and anthracene-containing polyspirobifluorene copolymers studied by the charge-generation layer time-of-flight technique," *J. Appl. Phys.* **99**, 033710 (2006).
90. F. Laquai, G. Wegner, and H. Bässler, "What determines the mobility of charge carriers in conjugated polymers?" *Philos. Trans. R. Soc. London Ser. A* **365**, 1473–1487 (2007).
91. G. Juška et al., "Extraction current transients: new method of study of charge transport in microcrystalline silicon," *Phys. Rev. Lett.* **84**, 4946–4949 (2000).

92. G. Juška et al., "Charge transport at low electric fields in π -conjugated polymers," *Phys. Rev. B* **65**, 233208 (2002).
93. A. Pivrikas et al., "A review of charge transport and recombination in polymer/fullerene organic solar cells," *Prog. Photovoltaics Res. Appl.* **15**, 677–696 (2007).
94. G. Dennler et al., "Charge carrier mobility and lifetime versus composition of conjugated polymer/fullerene bulk-heterojunction solar cells," *Org. Electron.* **7**, 229–234 (2006).
95. A. Kumar, H.-H. Liao, and Y. Yang, "Hole mobility in optimized organic photovoltaic blend films obtained using extraction current transients," *Org. Electron.* **10**, 1615–1620 (2009).
96. B. T. de Villers et al., "Improving the reproducibility of P3HT:PCBM solar cells by controlling the PCBM/cathode interface," *J. Phys. Chem. C* **113**, 18978–18982 (2009).
97. A. Pivrikas et al., "Comparative study of bulk and interface transport in disordered fullerene films," *Phys. Status Solidi B* **248**, 2656–2659 (2011).
98. G. Juška et al., "Charge-carrier transport and recombination in thin insulating films studied via extraction of injected plasma," *Phys. Rev. B* **74**, 115314 (2006).
99. G. Juška et al., "Double-injection current transients as a way of measuring transport in insulating organic films," *J. Appl. Phys.* **101**, 114505 (2007).
100. G. Juška et al., "Double injection in organic bulk-heterojunction," *J. Non-Cryst. Solids* **354**, 2858–2861 (2008).
101. Y. Yamashita, "Organic semiconductors for organic field-effect transistors," *Sci. Technol. Adv. Mater.* **10**, 024313 (2009).
102. Y. Guo, G. Yu, and Y. Liu, "Functional organic field-effect transistors," *Adv. Mater.* **22**, 4427–4447 (2010).
103. H. Usta, A. Facchetti, and T. J. Marks, "n-Channel semiconductor materials design for organic complementary circuits," *Acc. Chem. Res.* **44**, 501–510 (2011).
104. A. Facchetti, " π -conjugated polymers for organic electronics and photovoltaic cell applications," *Chem. Mater.* **23**, 733–758 (2011).
105. T. Okachi et al., "Influence of injection barrier on the determination of charge-carrier mobility in organic light-emitting diodes by impedance spectroscopy," *Thin Solid Films* **517**, 1331–1334 (2008).
106. G. Garcia-Belmonte et al., "Charge carrier mobility and lifetime of organic bulk heterojunctions analyzed by impedance spectroscopy," *Org. Electron.* **9**, 847–851 (2008).
107. M. A. Lampert and P. Mark, *Current Injection in Solids*, Academic Press, New York (1970).
108. A. Kokil, K. Yang, and J. Kumar, "Techniques for characterization of charge carrier mobility in organic semiconductors," *J. Polym. Sci. Part B Polym. Phys.* **50**, 1130–1144 (2012).
109. D. Poplavskyy and J. Nelson, "Nondispersive hole transport in amorphous films of methoxy-spirofluorene-arylamine organic compound," *J. Appl. Phys.* **93**, 341–346 (2003).
110. T. Chiba et al., "Hole mobility measurement of 4, 4'-bis [N-(1-naphthyl)-N-phenylamino]-biphenyl by dark injection method," *Chem. Phys. Lett.* **502**, 118–120 (2011).
111. A. J. Campbell et al., "Transient and steady-state space-charge-limited currents in polyfluorene copolymer diode structures with ohmic hole injecting contacts," *Appl. Phys. Lett.* **76**, 1734–1736 (2000).
112. T. Esward et al., "A metrology perspective on the dark injection transient current method for charge mobility determination in organic semiconductors," *J. Appl. Phys.* **109**, 093707 (2011).
113. P. Blom, M. De Jong, and M. Van Munster, "Electric-field and temperature dependence of the hole mobility in poly (p-phenylene vinylene)," *Phys. Rev. B* **55**, R656–R659 (1997).
114. V. D. Mihailetschi et al., "Compositional dependence of the performance of poly (p-phenylene vinylene): methanofullerene bulk-heterojunction solar cells," *Adv. Funct. Mater.* **15**, 795–801 (2005).
115. V. D. Mihailetschi et al., "Electron transport in a methanofullerene," *Adv. Funct. Mater.* **13**, 43–46 (2003).
116. V. Shrotriya et al., "Effect of self-organization in polymer/fullerene bulk heterojunctions on solar cell performance," *Appl. Phys. Lett.* **89**, 063505 (2006).

117. B. Chen et al., "Improved time-of-flight technique for measuring carrier mobility in thin films of organic electroluminescent materials," *Jpn. J. Appl. Phys.* **39**, 1190–1192 (2000).
118. R. De Boer et al., "Space charge limited transport and time of flight measurements in tetracene single crystals: a comparative study," *J. Appl. Phys.* **95**, 1196–1202 (2004).
119. V. Percec et al., "Self-organization of supramolecular helical dendrimers into complex electronic materials," *Nature* **419**, 384–387 (2002).
120. A. Kokil et al., "Charge carrier transport in poly(2,5-dialkoxy-p-phenylene ethynylene)s," *Synth. Met.* **138**, 513–517 (2003).
121. S. A. Choulis et al., "High ambipolar and balanced carrier mobility in regioregular poly(3-hexylthiophene)," *Appl. Phys. Lett.* **85**, 3890–3892 (2004).
122. K. Yang et al., "Determination of electron and hole mobility of regioregular poly(3-hexylthiophene) by the time of flight method," *J. Macromol. Sci. Part A* **44**, 1261–1264 (2007).
123. E. Hittinger, A. Kokil, and C. Weder, "Synthesis and characterization of cross-linked poly(p-phenylene ethynylene)s," *Macromol. Rapid Commun.* **25**, 710–715 (2004).
124. G. Li et al., "High-efficiency solution processable polymer photovoltaic cells by self-organization of polymer blends," *Nat. Mater.* **4**, 864–868 (2005).
125. G. Juška et al., "Charge transport in π -conjugated polymers from extraction current transients," *Phys. Rev. B* **62**, R16235 (2000).
126. S. Bange, M. Schubert, and D. Neher, "Charge mobility determination by current extraction under linear increasing voltages: case of nonequilibrium charges and field-dependent mobilities," *Phys. Rev. B* **81**, 035209 (2010).
127. K. Genevicius et al., "Separation of fast and slow transport in regiorandom poly(3-hexylthiophene)," *Synth. Met.* **137**, 1407–1408 (2003).
128. A. J. Mozer et al., "The effect of molecule size and shape on free charge generation, transport and recombination in all-thiophene dendrimer: fullerene bulk heterojunctions," *Org. Electron.* **11**, 573–582 (2010).
129. A. Pivrikas et al., "Meyer–Neldel rule for charge carrier transport in fullerene devices: a comparative study," *Org. Electron.* **12**, 161–168 (2011).
130. A. Baumann et al., "Influence of phase segregation on recombination dynamics in organic bulk-heterojunction solar cells," *Adv. Funct. Mater.* **21**, 1687–1692 (2011).
131. G. Juška et al., "Double injection as a technique to study charge carrier transport and recombination in bulk-heterojunction solar cells," *Appl. Phys. Lett.* **87**, 222110 (2005).
132. G. Sliužys et al., "Recombination of photogenerated and injected charge carriers in π -conjugated polymer/fullerene blends," *Thin Solid Films* **511**, 224–227 (2006).
133. D. Barbe and C. Westgate, "Surface state parameters of metal-free phthalocyanine single crystals," *J. Phys. Chem. Solids* **31**, 2679–2687 (1970).
134. J. Cabanillas-Gonzalez et al., "Photophysics of charge transfer in a polyfluorene/violanthrone blend," *Phys. Rev. B* **71**, 014211 (2005).
135. J. Müller et al., "Linewidth-limited energy transfer in single conjugated polymer molecules," *Phys. Rev. Lett.* **91**, 267403 (2003).
136. S. Meskers et al., "Time-resolved infrared-absorption study of photoinduced charge transfer in a polythiophene-methanofullerene composite film," *Phys. Rev. B* **61**, 9917–9920 (2000).
137. T. Agostinelli et al., "A planar organic near infrared light detector based on bulk heterojunction of a heteroquaterphenoquinone and poly[2-methoxy-5-(2'-ethyl-hexyloxy)-1,4-phenylene vinylene]," *J. Appl. Phys.* **104**, 114508 (2008).
138. T. J. Savenije et al., "Mobility and decay kinetics of charge carriers in photoexcited PCBM/PPV blends," *Phys. Rev. B* **69**, 155205 (2004).
139. P. Pingel et al., "Temperature-resolved local and macroscopic charge carrier transport in thin P3HT layers," *Adv. Funct. Mater.* **20**, 2286–2295 (2010).
140. T. J. Savenije et al., "Revealing the dynamics of charge carriers in polymer: fullerene blends using photoinduced time-resolved microwave conductivity," *J. Phys. Chem. C* **117**, 24085–24103 (2013).
141. L. Dhar, J. A. Rogers, and K. A. Nelson, "Time-resolved vibrational spectroscopy in the impulsive limit," *Chem. Rev.* **94**, 157–193 (1994).

142. C. Gautham et al., "Time-resolved two-photon excitation of long-lifetime polaritons," *Optica* **4**, 118–123 (2017).
143. T. Yamada et al., "Impact of photon recycling on carrier recombination processes in $\text{CH}_3\text{NH}_3\text{PbBr}_3$ single crystals revealed by time-resolved two-photon-excitation microscopy," *Lasers and Electro-Optics Europe and European Quantum Electronics Conf. (Conf. on CLEO/Europe-EQEC)*, pp. 1–1, IEEE (2017).
144. A. C. Breeson et al., "Phase quantification by x-ray photoemission valence band analysis applied to mixed phase TiO_2 powders," *Appl. Surf. Sci.* **423**, 205–209 (2017).
145. J. Halim et al., "X-ray photoelectron spectroscopy of select multi-layered transition metal carbides (MXenes)," *Appl. Surf. Sci.* **362**, 406–417 (2016).
146. J. Cabanillas-Gonzalez, G. Grancini, and G. Lanzani, "Pump-probe spectroscopy in organic semiconductors: monitoring fundamental processes of relevance in optoelectronics," *Adv. Mater.* **23**, 5468–5485 (2011).
147. G. Cerullo et al., "Time-resolved methods in biophysics. 4. Broadband pump-probe spectroscopy system with sub-20 fs temporal resolution for the study of energy transfer processes in photosynthesis," *Photochem. Photobiol. Sci.* **6**, 135–144 (2007).
148. J. Cabanillas-Gonzalez et al., "Photoinduced transient stark spectroscopy in organic semiconductors: a method for charge mobility determination in the picosecond regime," *Phys. Rev. Lett.* **96**, 106601 (2006).
149. C. J. Takacs et al., "Mapping orientational order in a bulk heterojunction solar cell with polarization-dependent photoconductive atomic force microscopy," *ACS Nano* **8**, 8141–8151 (2014).
150. R. Giridharagopal et al., "Submicrosecond time resolution atomic force microscopy for probing nanoscale dynamics," *Nano Lett.* **12**, 893–898 (2012).
151. D. C. Coffey and D. S. Ginger, "Time-resolved electrostatic force microscopy of polymer solar cells," *Nat. Mater.* **5**, 735–740 (2006).
152. J. Gao et al., "Polythiethylene-vinylene structure-function correlations revealed from resonance Raman spectroscopy and photocurrent imaging," *J. Phys. Chem. C* **119**, 8980–8990 (2015).
153. A. B. Naden, J. Loos, and D. A. MacLaren, "Structure-function relations in diF-TES-ADT blend organic field effect transistors studied by scanning probe microscopy," *J. Mater. Chem. C* **2**, 245–255 (2014).
154. E. Betzig et al., "Super-resolution imaging with near-field scanning optical microscopy (NSOM)," *Ultramicroscopy* **25**, 155–163 (1988).
155. C. M. Harris, "Product review: shedding light on NSOM," *Anal. Chem.* **75**, 223A–228A (2003).
156. C. J. Lombardo et al., "Scanning photocurrent microscopy of lateral organic bulk heterojunctions," *Phys. Chem. Chem. Phys.* **14**, 13199–13203 (2012).
157. A. J. Das, R. Shivanna, and K. Narayan, "Photoconductive NSOM for mapping optoelectronic phases in nanostructures," *Nanophotonics* **3**, 19–31 (2014).
158. J. M. Mativetsky, Y.-L. Loo, and P. Samorì, "Elucidating the nanoscale origins of organic electronic function by conductive atomic force microscopy," *J. Mater. Chem. C* **2**, 3118–3128 (2014).
159. L. S. Pingree, O. G. Reid, and D. S. Ginger, "Imaging the evolution of nanoscale photocurrent collection and transport networks during annealing of polythiophene/fullerene solar cells," *Nano Lett.* **9**, 2946–2952 (2009).
160. M. Dante, J. Peet, and T.-Q. Nguyen, "Nanoscale charge transport and internal structure of bulk heterojunction conjugated polymer/fullerene solar cells by scanning probe microscopy," *J. Phys. Chem. C* **112**, 7241–7249 (2008).
161. D. Moerman et al., "Towards a unified description of the charge transport mechanisms in conductive atomic force microscopy studies of semiconducting polymers," *Nanoscale* **6**, 10596–10603 (2014).
162. S. Uttiya et al., "Connecting molecule oxidation to single crystal structural and charge transport properties in rubrene derivatives," *J. Mater. Chem. C* **2**, 4147–4155 (2014).

163. D. Wood et al., “Quantitative nanoscale mapping with temperature dependence of the mechanical and electrical properties of poly (3-hexylthiophene) by conductive atomic force microscopy,” *J. Phys. Chem. C* **119**, 11459–11467 (2015).
164. L. V. Kelvin, “V. Contact electricity of metals,” *London Edinburgh Dublin Philos. Mag. J. Sci.* **46**, 82–120 (2009).
165. A. Liscio, V. Palermo, and P. Samorì, “Nanoscale quantitative measurement of the potential of charged nanostructures by electrostatic and Kelvin probe force microscopy: unraveling electronic processes in complex materials,” *Acc. Chem. Res.* **43**, 541–550 (2010).
166. V. Palermo, M. Palma, and P. Samorì, “Electronic characterization of organic thin films by Kelvin probe force microscopy,” *Adv. Mater.* **18**, 145–164 (2006).
167. I. Lange et al., “Correlation between the open circuit voltage and the energetics of organic bulk heterojunction solar cells,” *J. Phys. Chem. Lett.* **4**, 3865–3871 (2013).
168. K. Maturová et al., “Scanning Kelvin probe microscopy on bulk heterojunction polymer blends,” *Adv. Funct. Mater.* **19**, 1379–1386 (2009).
169. V. Palermo et al., “A Kelvin probe force microscopy study of the photogeneration of surface charges in all-thiophene photovoltaic blends,” *Adv. Funct. Mater.* **17**, 472–478 (2007).
170. L. Collins et al., “Quantitative 3D-KPFM imaging with simultaneous electrostatic force and force gradient detection,” *Nanotechnology* **26**, 175707 (2015).
171. R. Garcia and E. T. Herruzo, “The emergence of multifrequency force microscopy,” *Nat. Nanotechnol.* **7**, 217–226 (2012).
172. K. R. Rajesh et al., “Design of organic ternary blends and small-molecule bulk heterojunctions: photophysical considerations,” *J. Photonics Energy* **5**, 057208 (2015).
173. P. Irkhin and I. Biaggio, “Direct imaging of anisotropic exciton diffusion and triplet diffusion length in rubrene single crystals,” *Phys. Rev. Lett.* **107**, 017402 (2011).
174. P. Deotare et al., “Nanoscale transport of charge-transfer states in organic donor–acceptor blends,” *Nat. Mater.* **14**, 1130–1134 (2015).
175. N. Rawat et al., “Macroscopic molecular ordering and exciton delocalization in crystalline phthalocyanine thin films,” *J. Phys. Chem. Lett.* **6**, 1834–1840 (2015).
176. S. Sharifzadeh et al., “Relating the physical structure and optoelectronic function of crystalline TIPS-pentacene,” *Adv. Funct. Mater.* **25**, 2038–2046 (2015).

Chengxi Zhang received his MS degree in materials engineering from Chongqing University of Technology in 2016. He is currently a research assistant in Dr. Hsien-Yi Hsu’s group at the City University of Hong Kong. His research interests include photophysics, electrochemistry, and photoelectrochemistry of organic and inorganic photovoltaic devices.

Rugeng Liu is a PhD candidate in the School of Energy and Environment of the City University of Hong Kong. He received his BS degree from the School of Chemical Engineering and Technology from Tianjin University, Tianjin, China, in 2013 and his MS degree from China University of Petroleum (Beijing) in Beijing, China, in 2016. His research interests mainly focus on synthesis and characterization of perovskites for optoelectronic devices.

Chun Hong Mak received his BS degree in natural sciences from Chinese University of Hong Kong, China, in 2017. He is currently a research assistant in Dr. Hsien-Yi Hsu’s group at the City University of Hong Kong. His research interests include the study of photophysical and electrochemical properties for macromolecular organic assemblies and hybrid organic–inorganic perovskite materials in the application of solid-state solar cells and solar fuels.

Xingli Zou received his PhD from Shanghai University (SHU) in 2012. He joined the State Key Laboratory of Advanced Special Steel, SHU, as a postdoctoral fellow from 2012 to 2014 and then joined the Laboratory and School of Materials Science and Engineering, SHU, as an associate professor in 2015. He joined the University of Texas at Austin as a research fellow in 2017. His research involves the design and synthesis of materials for energy applications.

Hsin-Hui Shen completed her PhD in physical chemistry at Oxford University in 2008. Following that, she commenced her postdoctoral research at CSIRO (2008 to 2011) and received the ARC Super Science Research Fellowship at Monash University (2012 to 2015). In 2016, she

received an NHMRC Career Development Fellowship. She is a physical scientist who can transit between two diverse worlds of physics and microbial infections with ease.

Shao-Yuan Leu is an assistant professor in the Civil and Environmental Engineering Department at the Hong Kong Polytechnic University. His research is on applying material and organic chemistry in resolving energy problems in urban environments. He obtained his BS degree from the National Taiwan University and his PhD from UCLA. He was a licensed professional engineer in California and a postdoc in the USDA Forest Products Lab (Madison). He has authored 31 peer-reviewed papers since 2009.

Li Ji received his BS degree from Xiamen University in 2011 and his PhD in electrical engineering from the University of Texas at Austin in 2016. Currently, he is a research associate at Microelectronics Research Center at the University of Texas at Austin. His research interests include electronic and optoelectronics semiconductor devices, renewable energy, photoelectrochemistry, and photophysics.

Hsien-Yi Hsu is an assistant professor in the School of Energy and Environment at City University of Hong Kong. He earned his PhD from the University of Florida with a focus on photophysics of platinum acetylide polymers. His research interests involve the material design, synthesis, processing, imaging, spectroscopy, and solar energy application, aiming to explore photophysics and photoelectrochemistry of hybrid perovskite semiconductors and functional metallopolymer materials for developing efficient and stable solar energy conversion processes.